
Demystifying Mergeability: Interpretable Properties to Predict Model Merging Success

Luca Zhou¹ Bo Zhao² Rose Yu² Emanuele Rodolà^{1,3}

Abstract

Model merging combines knowledge from separately fine-tuned models, yet success factors remain poorly understood. While recent work treats mergeability as an intrinsic property, we show with an architecture-agnostic framework that it fundamentally depends on both the merging method and the partner tasks. Using linear optimization over a set of interpretable pairwise metrics (e.g., gradient L_2 distance), we uncover properties correlating with post-merge performance across four merging methods. We find substantial variation in success drivers (46.7% metric overlap; 55.3% sign agreement), revealing method-specific “fingerprints”. Crucially, however, *subspace overlap* and *gradient alignment* metrics consistently emerge as foundational, method-agnostic prerequisites for compatibility. These findings provide a diagnostic foundation for understanding mergeability and motivate future fine-tuning strategies that explicitly encourage these properties.

1. Introduction

Model merging has emerged as a practical approach for combining knowledge across multiple fine-tuned neural networks without retraining. Given multiple task-specific fine-tuned models, merging aims to produce a single model that performs well on multiple tasks simultaneously. This is particularly valuable in settings where computational resources are limited or where a unified model is preferred over task-specific checkpoints.

Despite its practical appeal, model merging remains highly unpredictable. Some model pairs merge seamlessly, yielding performance close to the average of their individual task accuracies. Others suffer catastrophic performance degradation due to task interference. This inconsistency motivates

¹Sapienza University of Rome ²UC San Diego ³Paradigma. Correspondence to: Luca Zhou <luca.zhou@uniroma1.it>.

a fundamental question: *what determines the compatibility between models when merged?*

Recent work (Rahamim et al., 2026) has proposed that mergeability is an intrinsic property of individual models: if a model is mergeable, it remains so regardless of its merge partner, and they do not explore multiple merge algorithms. Under this view, the challenge reduces to identifying and certifying models with high mergeability potential. Complementary to this framing, we note that this perspective implicitly aggregates multiple sources of variation, including the properties of both merged models and the choice of merge algorithm, into a single scalar notion of mergeability. Consequently, it remains unclear how compatibility patterns may change across different merging methods or partners.

We test this hypothesis using a flexible, architecture- and method-agnostic framework that applies linear optimization over extensible sets of interpretable pairwise metrics. This approach serves as a scientific probe to isolate the geometric and functional properties associated with model compatibility, revealing how these requirements shift across merging mechanisms (see Figure 1). We emphasize that our goal is not to maximize predictive performance, but rather to **unveil the underlying signals of successful merging**.

Applied to four representative merge methods, namely Task Arithmetic (TA) (Ilharco et al., 2023), Weight Averaging (WA) (Wortsman et al., 2022), Task Singular Vector (TSV) merging (Gargiulo et al., 2024), and Isotropic merging (ISO) (Marczak et al.), using 28 pairwise metrics spanning weight-space, activation-, and gradient-based measures, our analysis reveals that each merging method exhibits a distinct “success fingerprint”. The substantial variation in optimized coefficients (20–80% metric overlap and 36–75% sign agreement) demonstrates that mergeability is not a static and intrinsic model property but a dynamic, method-dependent relationship. Notably, the same metric can even exert opposite effects across different merging methods.

Our framework delivers three core advantages. First, **predictive structure**: by optimizing for generalization under leave-one-task-out evaluation, the framework makes testable predictions about merging outcomes on unseen tasks and model pairs, rather than providing post-hoc explanations

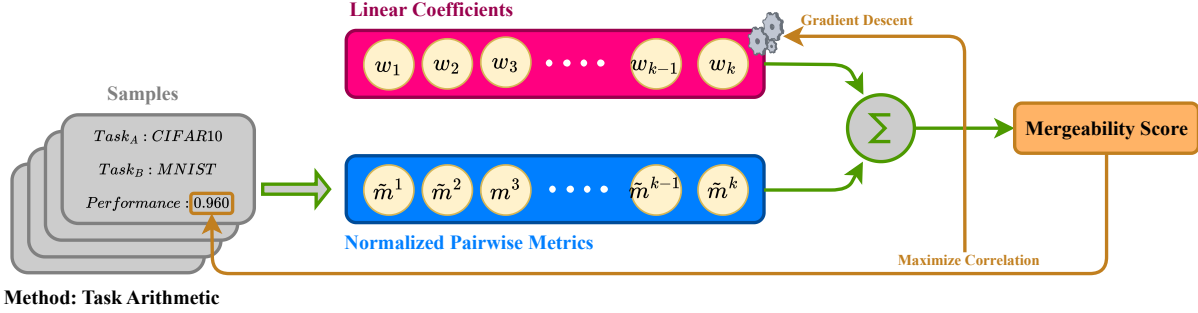


Figure 1. Linear optimization procedure of metric coefficients to maximize the Pearson correlation with the true post-merge performance. Repeated for all methods, yielding per-method optimal coefficients. Green and orange depict the forward and backward flows, respectively.

alone. Second, **full interpretability**: unlike black-box predictors (Bolton et al., 2026), transparent coefficients reveal which model properties are predictive of success for each merging method. Third, **flexibility**: the same optimization can be applied to new merge algorithms or architectures, enabling practitioners to identify and target the properties most associated with successful merging. Finally, we demonstrate the actionability of our framework through a toy experiment, where insights derived from our analysis directly motivate a fine-tuning strategy that improves mergeability. Our contributions are summarized as:

1. **Deconstructing the Nature of Mergeability:** We introduce an interpretable architecture-agnostic approach that uses linear optimization as a diagnostic tool to identify pairwise model properties that correlate with merging success across merging methods, moving beyond the “intrinsic mergeability” hypothesis.
2. **Discovery of Method-Specific Success Fingerprints:** We demonstrate that while mergeability requirements are highly method-dependent, subspace and gradient alignments serve as foundational, method-agnostic signals of universal model compatibility.
3. **Actionable and Extensible:** Linear models achieve meaningful prediction ($r \in [0.34, 0.61]$, $p < 0.01$) with full transparency vs. black-box approaches. Practitioners can apply our framework to any new method/architecture to identify key properties to encourage during fine-tuning for enhanced mergeability, as we show in a toy experiment.

2. Related Work

Model merging and task vectors. Model merging aims to combine multiple models into one without additional joint training and adaptation. The purpose of model merging can be two-fold: i) merging models trained on the same task can enhance robustness (Crisostomi et al., 2024), while ii) merging models trained on different tasks enables multi-task capabilities (Li et al., 2023). This work focuses on the

latter setting. Prior work has explored simple parameter-space operators such as linear interpolation (Wortsman et al., 2022; Frankle et al., 2020), task vector arithmetic (Ilharco et al., 2023), as well as more structured variants that account for layer-wise geometry and task interference (Yadav et al., 2023; Zhou et al., 2025b; Davari & Belilovsky, 2023; Deep et al., 2024; Wang et al., 2024a). Task-vector-based methods view fine-tuning as learning a displacement in weight space and study how these displacements can be composed to transfer or combine capabilities across tasks. More recent approaches refine this view by connecting task vectors to gradients (Zhou et al., 2025a; Daheim et al., 2024), and exploit the low-rank structure of weight matrices (Gargiulo et al., 2024; Marczak et al.). For example, methods based on Task Singular Vectors (TSVs) decompose layer-wise task updates and explicitly reduce inter-task interference before merging, achieving stronger performance than naive arithmetic combinations. These works highlight that different merge operators implicitly rely on different geometric assumptions about how task updates interact.

Intrinsic mergeability. A recent line of work seeks to explain *why* some models are more easily merged than others by introducing explicit notions of “mergeability”. In particular, Rahamim et al. (2026) define a mergeability score based on repeated merge-and-evaluate trials with random partners, concluding that mergeability can be treated as an intrinsic property, primarily governed by the base model’s prior knowledge. In this view, a highly mergeable model is expected to remain so across different merge partners.

In this work, we adopt a complementary perspective. Rather than treating mergeability as a partner-independent scalar, we examine how the properties predictive of merging success depend on the choice of merge algorithm and vary across merge partners. Additionally, instead of inferring mergeability solely from black-box evaluation trials, we analyze a set of interpretable pairwise metrics to characterize the factors associated with successful merging. This enables a more granular analysis that moves beyond identifying *whether* a model is mergeable to understanding *under which*

Table 1. Summary of mergeability metrics by category.

Category	Metrics	Count
Task Vector	cos sim, L_2 dist, dot, angle, magnitude ratio	5
Effective Rank	eff rank, stable rank, spectral gap, SV ratio	7
Subspace Overlap	SV overlap, subspace overlap, interaction	6
Activation-Based	L_2 dist, cosine sim, magnitude ratio, dot	4
Gradient-Based	encoder/input grad, L_2 dist., cos sim, dot	6
Total		28

conditions and by which signals compatibility arises.

Predicting merge outcomes from similarity signals. Another strand of work explores using similarity signals to predict merge outcomes (Yang et al., 2023; Matena & Rafel, 2022), with works like Bolton et al. (2026) employing black-box models to optimize operator selection and merge orders. While these approaches demonstrate the predictive utility of similarity metrics, they prioritize performance over an understanding of the underlying signals.

In contrast, we treat pre-merge signals as a *discovery mechanism*. By optimizing linear combinations of 28 pairwise metrics, we prioritize transparency over non-linear complexity to identify properties driving success across merging methods. While our framework matches an MLP baseline’s predictive performance, its primary value lies in the explicit coefficients revealing method-specific mergeability signals.

3. Mergeability Metrics

We introduce a suite of 28 expandable pairwise metrics to study model compatibility. Since no single metric is sufficiently predictive (A.1), we leverage their combined expressivity to characterize mergeability. These metrics are computed without performing the merge, enabling efficient pre-screening of model pairs. For layer-wise metrics, we report the mean across all layers. We categorize these metrics into the following five groups (detailed definitions in A.4).

3.1. Task Vector Geometry Metrics

Given two task vectors $\tau_A, \tau_B \in \mathbb{R}^D$, defined as the flattened 1D difference vector between fine-tuned and pre-trained weights, we examine their geometric relationship in weight space. The intuition is that task vectors pointing in similar directions may interfere less during merging.

- **Dot Product & Cosine Similarity:** Measure the directional alignment between task vectors, with and without magnitude consideration.
- **L_2 Distance:** Smaller values indicate similar updates.
- **Angle:** The directional difference in degrees.
- **Magnitude Ratio:** The ratio between task vector magnitudes; a value near 1 suggests balanced contributions.

3.2. Effective Rank Metrics

Recent work suggests that Task Arithmetic benefits from low-rank task vectors (Liu et al., 2025). We analyze this property using the singular values $\sigma_1 \geq \sigma_2$ of the $2 \times D$ matrix $\mathbf{T} = [\tau_A; \tau_B]^\top$ formed by the two task vectors.

- **Effective Rank (Global/Layer-wise):** Measures singular value entropy; a value of 1 indicates low-rank alignment, while higher values suggest diffuse, conflicting subspaces. Layer-wise results are averaged across layers, weighted by the update magnitudes.
- **Effective Rank Score (Global/Layer-wise):** A normalized version of the effective rank mapping values to $[1, 0]$, where higher scores benefit compatibility.
- **Stable Rank:** An alternative dimensionality measure based on the singular values’ squared Frobenius norm.
- **Spectral Gap:** The normalized difference between singular values; a large gap indicates a single dominant direction, suggesting strong alignment.
- **Singular Value Ratio:** The ratio σ_2/σ_1 , where smaller values signify stronger alignment.

3.3. Subspace Overlap Metrics

These metrics analyze how the principal directions modified by each task relate to one another, utilizing the Singular Value Decomposition (SVD) of individual $2D$ weight matrices to extract left (U) and right (V) singular vectors. Non- $2D$ parameters, such as biases, are ignored.

- **Singular Value Overlap:** The cosine similarity between the top-100 normalized singular value distributions, providing a measure of spectral similarity averaged across layers.
- **Left Subspace Overlap:** Measures the alignment between the top- k left singular vectors using the Frobenius norm of their product; we set $k = 10$ here and in subsequent metrics.
- **Right Subspace Overlap (Top- k and Bottom- k):** Measures overlap between the strongest and weakest right singular vectors, as different merging methods may be sensitive to different spectral components.
- **Interaction Matrix Overlap (Top- k and Bottom- k):** Analyzes the principal angles between subspaces by reporting the mean squared singular value of the interaction matrix formed by the right singular vectors.

3.4. Activation-Based Metrics

To complement weight-space analysis with functional insights, we measure how similarly models process identical inputs. We use a calibration set \mathcal{D}_{cal} (10 random samples per task) to extract activations from the final encoder layer.

- **Activation L_2 Distance:** The Euclidean distance between mean activations across calibration samples.
- **Activation Cosine Similarity:** The directional alignment of mean activation vectors.
- **Activation Magnitude Ratio:** The ratio of activation norms, indicating consistency in feature scales.
- **Activation Dot Product:** A combined measure of direction and magnitude for activation alignment.

3.5. Gradient-Based Metrics

Gradient alignment often correlates with multitask learning success (Yu et al., 2020). With task-specific calibration data (10 random samples per task), we measure gradient similarity at two levels:

Encoder Gradient Metrics. Measure the similarity of loss gradients with respect to encoder parameters:

- **Encoder Gradient Cosine Similarity:** Measures the alignment of directions in which models require parameter updates.
- **Encoder Gradient L_2 Distance:** The Euclidean magnitude of the difference between gradient vectors.
- **Encoder Gradient Dot Product:** Captures joint directional and magnitude agreement.

Input Gradient Metrics. Capture how models attend to input features by computing gradients with respect to input images:

- **Input Gradient Cosine Similarity:** Determines whether models focus on similar input regions.
- **Input Gradient L_2 Distance:** Quantifies the magnitude of input sensitivity differences.
- **Input Gradient Dot Product:** A combined measure of direction and magnitude for saliency alignment.

Table 1 summarizes all 28 metrics and their computational requirements. Weight-based and effective rank metrics require only the task vectors and are thus the most efficient. Activation and gradient metrics require a small calibration set and forward/backward passes, but capture functional properties that pure weight-space metrics may miss.

4. Methodology

To assess the predictive power of multi-metric combinations, we optimize a linear model to maximize the Pearson correlation between a predicted score and actual post-merge performance. Specifically, for $K = 28$ normalized metrics $\tilde{m}_{ij}^{(k)}$, we seek coefficients $\mathbf{w} = (w_1, \dots, w_K)^\top$ such that

the score

$$\hat{s}_{ij} = \sum_{k=1}^K w_k \cdot \tilde{m}_{ij}^{(k)} \quad (1)$$

best aligns with the post-merge performance p_{ij} . Figure 1 depicts the overall optimization procedure.

Each training sample is a tuple $\langle \mathcal{T}_A, \mathcal{T}_B, F, y \rangle$, representing task A , task B , the merge method, and the resulting post-merge performance. While we explored non-linear alternatives like MLP (Appendix A.2), the linear approach proved superior in both stability and interpretability, especially given the limited and noisy nature of the dataset. This framework allows us to isolate the contribution of each metric while maintaining predictive reliability.

Metric Normalization. To ensure fair contribution to the linear combination, we apply min-max normalization to map all metrics to the range $[-1, 1]$ to account for varying original scales (e.g., bounded cosine similarity vs. unbounded L_2 distances). Minima and maxima are computed across the training data to avoid data leakage during validation.

Optimization Objective. We formulate the coefficient learning problem as maximizing the Pearson correlation coefficient between predicted mergeability scores and observed post-merge performance p :

$$\mathbf{w}^* = \arg \max_{\mathbf{w}} r(\mathbf{X}\mathbf{w}, \mathbf{p}) \quad \text{subject to} \quad \sum_{k=1}^K w_k = 1 \quad (2)$$

where $\mathbf{p} \in \mathbb{R}^N$ is the vector of average classification accuracies of the merged model across the two tasks A and B , relative to individual models (i.e., $\frac{1}{2}[\frac{\text{acc}_{\text{merge}, A}}{\text{acc}_A} + \frac{\text{acc}_{\text{merge}, B}}{\text{acc}_B}]$), $\mathbf{X} \in \mathbb{R}^{N \times K}$ is the matrix of normalized metrics for N model pairs, and $r(\cdot, \cdot)$ denotes the Pearson correlation.

The sum-to-one constraint fixes an affine degree of freedom in the linear combination, ensuring identifiable coefficients that represent relative metric contributions. Since individual weights remain unbounded in magnitude, the formulation naturally captures both strong positive and negative correlations, effectively accommodating both metrics that are negatively and positively correlated with compatibility.

We optimize for Pearson correlation rather than MSE because our goal is to *rank* task pairs by mergeability, not to predict exact accuracies. Correlation is scale-invariant, which is desirable since the linear combination of features lives on an arbitrary scale, while accuracies lie in a narrow range. Optimizing MSE would entangle learning the correct ordering with matching this scale. In contrast, high correlation directly reflects the ranking quality practitioners care about: given candidate task pairs, which should be merged first? It also yields a single interpretable metric, the correlation coefficient r , summarizing how much variance in merge outcomes is explained by the learned combination.

Optimization Procedure. The coefficients are optimized via Adam (Kingma & Ba, 2014) and rescaled after each update to satisfy the sum-to-one constraint, ensuring that weights represent relative predictive contributions. We use early stopping with a patience of 50 iterations, halting when the improvement in training correlation falls below 10^{-4} .

Leave-One-Task-Out Cross-Validation. A key challenge in evaluating mergeability prediction is ensuring that the learned coefficients generalize to unseen task combinations. Simple random train-validation splits may still contain pairs involving tasks seen during training, leading to optimistic estimates. To address this, we employ *leave-one-task-out* (LOTO) cross-validation.

Let $\mathcal{T} = \{T_1, \dots, T_M\}$ denote the set of M tasks. In each fold f , we hold out all pairs involving task T_f :

$$\mathcal{V}_f = \{(i, j) : T_i = T_f \text{ or } T_j = T_f\} \quad (3)$$

The remaining pairs form the training set \mathcal{S}_f . We optimize coefficients \mathbf{w}_f on \mathcal{S}_f and evaluate on \mathcal{V}_f . This ensures that the validation pairs involve at least one task never seen during training, providing a rigorous test of generalization to novel task combinations.

For M tasks with $\binom{M}{2}$ total pairs, each fold holds out the $M - 1$ pairs involving the held-out task. We report: (i) *per-fold metrics*, including training and validation correlations for each fold; and (ii) *average coefficients*, $\bar{\mathbf{w}} = \frac{1}{M} \sum_{f=1}^M \mathbf{w}_f$ with standard deviations, to identify metrics that consistently contribute to prediction across folds.

This cross-validation scheme is more stringent than random splitting: rather than testing on random held-out pairs (which may involve familiar tasks in new combinations), we test on pairs where at least one task is entirely novel. High validation correlation under LOTO provides strong evidence that the learned metric combination captures genuine mergeability signals rather than task-specific artifacts.

5. Experimental Setup

Tasks and Models. Following Gargiulo et al. (2024), we evaluate our mergeability discovery framework on a benchmark of 20 diverse image classification tasks, with references in Appendix A.9: SUN397, Stanford Cars, RESISC45, EuroSAT, SVHN, GTSRB, MNIST, DTD, Flowers102, PCAM, FER2013, OxfordIIITPet, STL10, CIFAR10, CIFAR100, Food101, FashionMNIST, EMNIST, KMNIST, and RenderedSST2. We fine-tune CLIP ViT-B/16 encoders (Radford et al., 2021) for each task, initializing from OpenAI pretrained weights (see Appendix A.8.5). This yields 20 task-specific models, from which we extract task vectors $\boldsymbol{\tau}_i = \boldsymbol{\theta}_i - \boldsymbol{\theta}_0$ for each task i . The $\binom{20}{2} = 190$ unique model pairs form our dataset.

Merge Methods. We evaluate four representative merging

methods that span different algorithmic approaches:

- Task Arithmetic:** Adds scaled task vectors to the pre-trained model: $\boldsymbol{\theta}_{\text{merged}} = \boldsymbol{\theta}_0 + \lambda(\boldsymbol{\tau}_A + \boldsymbol{\tau}_B)$.
- Weight Averaging:** Simple average of fine-tuned weights: $\boldsymbol{\theta}_{\text{merged}} = \frac{1}{2}(\boldsymbol{\theta}_A + \boldsymbol{\theta}_B)$.
- Task Singular Vectors (TSV):** Orthogonalizes overlapping task singular directions in task vectors to minimize interference.
- Isotropic Merging:** Enforces a flattened singular value spectrum in a shared task-vector subspace.

Sparsity and Feature Selection. To assess stability and address potential multicollinearity, we supplement our primary analysis with L_1 (Lasso) regularization. This sparse approach distills the metrics into a minimal set of fundamental drivers, verifying whether the “success fingerprints” are authentic signals or artifacts of redundancy. The full optimization objective and details are in Appendix A.6.

6. Results

6.1. Predictive Mergeability

Upon optimizing the linear coefficients for all 20 folds with gradient descent, we obtain the LOTO cross-validation results for each method, as reported in Table 2. We report the per-fold statistics: mean and standard deviation across the 20 folds, of the Pearson correlation between the predicted post-merge performance and the actual performance. Figure 2 shows each metric category’s average per-metric contribution across methods. Normalization by category size ensures equitable comparison regardless of the number of metrics per category. The actual learned coefficients of the linear optimization are shown in A.3. Below, we discuss our observations that emerged from these results.

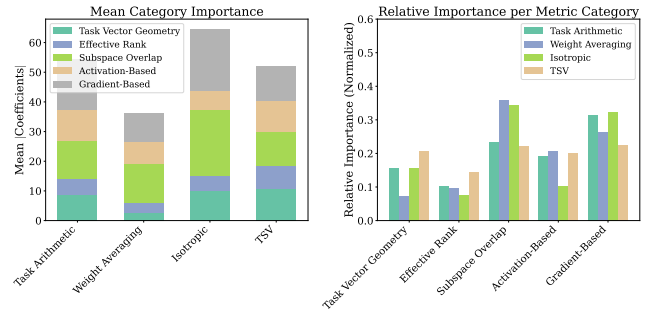


Figure 2. Comparison of metric category importance, normalized by the number of constituent metrics to account for varying category sizes. **Left:** Stacked bar chart showing the mean absolute coefficient magnitude per category for each merging method. **Right:** Grouped bar chart illustrating the relative importance of each category per method, demonstrating the proportional influence of a typical metric within each category.

Table 2. Leave-one-task-out cross-validation results. Statistics show mean \pm std of Pearson correlation r across 20 folds for the training and validation sets.

Method	Per-Fold Pearson Correlation (r)	
	Train (mean \pm std)	Val (mean \pm std)
Task Arithmetic	0.510 ± 0.099	0.343 ± 0.165
Weight Averaging	0.706 ± 0.090	0.555 ± 0.165
Isotropic	0.434 ± 0.089	0.328 ± 0.227
TSV	0.713 ± 0.167	0.572 ± 0.236

Predictability varies across methods. TSV merging exhibits the highest predictability, with a mean validation correlation of 0.572. Weight averaging follows with $r_{\text{val}} = 0.555$. In contrast, Task Arithmetic and Isotropic merging show lower and similar validation correlations.

Generalization gap. All methods show a gap between training and validation correlations, which is expected given that LOTO tests on entirely novel task combinations. The gap is smallest for TSV ($0.713 \rightarrow 0.572$, a 20% relative decrease) and largest for Task Arithmetic ($0.51 \rightarrow 0.343$, a 33% decrease), suggesting that TSV’s mergeability is governed by more generalizable principles.

6.2. Per-Method Metric Contributions

A core finding is that different merging methods rely on substantially different metrics for prediction, although subspace overlap and gradient-based metrics consistently exhibit the highest normalized contribution (See Fig.2 (right)). Table 3 shows the per-method top-5 metrics by average coefficient magnitude, while Figure 3 provides the full picture of the learned coefficients for all methods, highlighting their disparities. We defer the explicit values of the average learned coefficients to Appendix A.3, where we also detail metric overlap and coefficient sign agreement among the methods.

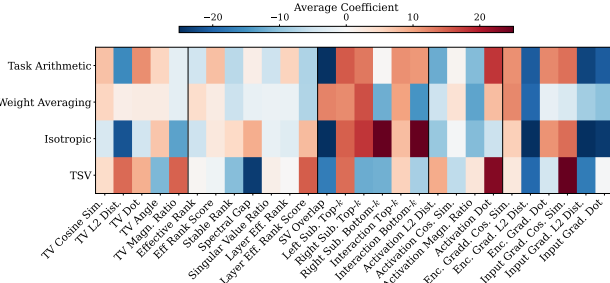


Figure 3. Per-method learned coefficients for all 28 metrics, averaged across the 20 leave-one-task-out folds.

Method-specific Patterns. For Task Arithmetic, negative signs for singular value overlap and gradient distances reveal a high sensitivity to model divergence, while positive correlation with activation dot product suggests that success requires aligned activation patterns. Weight Averaging similarly penalizes

Table 3. Descendingly sorted Top-5 metrics by average coefficient magnitude ($|\bar{w}|$) for each merging method. Signs indicate whether higher metric values predict better (+) or worse (-) mergeability.

Method	Metric	Sign
Task Arithmetic	Singular Value Overlap	-
	Input Grad. L_2 Distance	-
	Input Grad. Dot Product	-
	Encoder Grad. L_2 Distance	-
	Activation Dot Product	+
Weight Averaging	Encoder Grad. L_2 Distance	-
	Right Subspace Overlap Top- k	+
	Interaction Overlap Bottom- k	-
	Activation Mag. Ratio	-
	Singular Value Overlap	+
Isotropic	Input Grad. L_2 Distance	-
	Right Subspace Overlap Bottom- k	+
	Encoder Grad. L_2 Distance	-
	Interaction Overlap Bottom- k	+
	Singular Value Overlap	-
TSV	Input Grad. Cosine Sim.	+
	Spectral Gap	-
	Activation Dot Product	+
	Encoder Grad. L_2 Distance	-
	Input Grad. L_2 Distance	-

gradient distance but benefits significantly from right subspace overlap Top- k and singular value overlap, indicating that principal component alignment is more critical for simple averaging than for vector-based arithmetic. Isotropic merging is uniquely influenced by interaction overlap bottom- k , highlighting the role of small feature interactions in its stability. Finally, TSV relies on input gradient cosine Similarity and spectral gap, performing best when models agree on feature importance directions and maintain specific internal singular value distributions.

Subspace and gradient metrics serve as consistently important predictors across all four merge methods, with gradient-based and subspace overlap measures emerging as stable indicators of mergeability. Specifically, gradient measures such as input gradient L_2 distance and encoder gradient L_2 distance consistently yield negative coefficients, reinforcing the observation that larger gradient discrepancies align with poorer merge outcomes (Daheim et al., 2024). Simultaneously, the persistent predictive power of subspace overlap metrics across methods underscores the necessity of low-rank structural similarity in the weights learned by different models.

These results suggest that successful merging depend both on optimization dynamics and representational geometry.

High coefficient variance across folds. The standard deviations of learned coefficients are often large relative to their means (see Appendix 9), indicating that the optimal metric weighting varies depending on which task is held out, further highlighting that mergeability is not intrinsic to a model but depends on the merge partner. This instability suggests

Table 4. Stable predictive metrics and their average coefficients.

Metric	WA	TA	TSV	ISO	Avg
Encoder Grad. L_2 Distance	-19.6	-20.8	-19.5	-33.3	-23.3
Encoder Grad. Cosine Sim.	+12.1	+11.4	+2.7	+6.0	+8.1
Input Grad. L_2 Distance	-8.7	-23.0	-17.6	-36.3	-21.4
Input Grad. Dot Product	-10.3	-20.9	-0.2	-24.0	-13.9
Left Subspace Overlap Top- k	+11.8	+15.4	+14.0	+15.0	+14.1
Interaction Overlap Top- k	+10.1	+11.5	+5.8	+7.7	+8.8

that while a linear combination can predict mergeability within a fixed task distribution, the specific weighting may not transfer robustly to entirely new task domains.

Takeaway. These findings demonstrate that *mergeability is method-dependent*: a model may exhibit high compatibility with one partner yet prove incompatible with another, and the same pair of models may be highly compatible under one merging algorithm but entirely incompatible under another. Consequently, mergeability requires method-specific signals rather than a universal compatibility score. This motivates our investigation in the following section into whether certain metrics exhibit stable predictive power across methods.

6.3. Stable Metrics

While we just showed that optimal metric weightings are method-dependent, we now examine whether certain metrics exhibit *stable* predictive behavior across all merging methods. We define a stable metric as one whose average coefficient maintains a consistent sign across all four methods, indicating compatibility principles that transcend specific merging algorithms. To identify such metrics, we analyze the average coefficients \bar{w}_k and their standard deviations σ_k over the 20 LOTO folds for each method; metrics satisfying the sign-consistency criterion are reported in Table 4.

Gradient Distance as a Consistent Indicator. The most striking stable metric is encoder gradient L_2 distance, which carries a strong negative coefficient across all four methods (averaging -23.3). This indicates that *models with similar encoder gradients merge better*, regardless of the merging algorithm. The encoder gradient captures how each model’s loss responds to the encoder’s representation; similarity in this response suggests that the models have learned compatible representations. Similarly, input gradient L_2 distance is also consistently negative (averaging -21.4), hinting that models with similar input gradients merge better. This metric measures the difference in how each model’s loss responds to the input perturbations. This result is consistent with Daheim et al. (2024), where merging failure is associated with gradient mismatch. Interestingly, while smaller L_2 distances enhance mergeability, cosine similarity and dot product present mixed results, suggesting that the role of angles between gradients is more subtle, as a smaller angle implies

better alignment but also more interference, while orthogonal gradients are not aligned but interfere less.

Subspace Alignment Promotes Compatibility. Two subspace-based metrics show stable positive coefficients: left subspace overlap top- k and interaction matrix overlap top- k . These measure alignment between the principal directions modified by each task vector. The consistency of top- k (rather than bottom- k) subspace metrics suggests that alignment in the most dominant directions, those capturing the largest weight displacements, matters more than the alignment of the least significant directions for mergeability. This corroborates the observations in TSV, where interference occurs primarily when tasks compete for the same high-impact parameter subspaces.

Interpreting Stable Metrics Through the Lens of Task Interference. The stable metrics can be unified under the concept of *task interference*. Model merging fails when the combined task vectors interfere destructively (Yadav et al., 2023; Daheim et al., 2024; Wang et al., 2024b; Deep et al., 2024; Zhou et al., 2025a), either by pointing in opposing directions or by competing for the same representational capacity (Yang et al., 2024). Our stable metrics capture complementary aspects of this interference:

- **Gradient metrics** measure functional interference: do the tasks require conflicting parameter updates?
- **Subspace metrics** measure structural interference: do the tasks modify overlapping or orthogonal directions in weight space?

Low gradient distance, high alignment, and high subspace overlap indicate that tasks have learned compatible solutions using similar mechanisms, the ideal scenario for merging.

Practical Implications. The existence of stable metrics has important practical implications:

- i) **Method-Agnostic Screening:** Before selecting a merging algorithm, practitioners can compute the stable metrics to assess whether two models satisfy fundamental compatibility constraints. Low input gradient L_2 distance and high right subspace overlap top- k indicate that the pair avoids severe task interference and is therefore *eligible* for successful merging under most methods. However, because mergeability is method-dependent, these stable metrics should be interpreted as necessary but not sufficient conditions: satisfying them does not guarantee strong merge performance, but not satisfying them leads to severe degradation.
- ii) **Training Guidance:** The importance of gradient-based metrics suggests that fine-tuning procedures that promote gradient similarity across tasks (e.g., via explicit

regularization or shared optimization trajectories) benefit model mergeability. When the merging method is known *a priori*, one could enforce method-specific constraints during fine-tuning to improve compatibility. We discuss a proof-of-concept experiment next.

Enhancing Mergeability during fine-tuning. To demonstrate the actionability of our findings, we conduct a *toy experiment* motivated by the importance of gradient distance. We fine-tune task-specific models with a gradient-magnitude penalty, encouraging smaller parameter updates and keeping models closer to the pretrained solution. Operating within a shared loss basin naturally promotes gradient alignment. Consistent with this intuition (Ortiz-Jimenez et al., 2024; Zhou et al., 2025a), the regularized models are more mergeable, yielding a modest but consistent improvement in post-merge performance ($\Delta = +0.55$). See Appendix A.5 for details. We emphasize that this experiment serves as a proof of concept; more principled fine-tuning strategies, targeting multiple signals and specific merging methods, are expected to yield larger gains.

7. Ablations

7.1. Stability of Discovery via L_1 Distillation

To assess the robustness of the discovered success fingerprints, we repeat the linear optimization with L_1 regularization to promote sparsity and reduce variance. As shown in Table 13 (Appendix A.6), the L_1 -regularized model achieves higher validation correlations and lower variance ($r \in [0.45, 0.66]$, $std \in [0.135, 0.199]$) compared to the dense formulation ($r \in [0.33, 0.71]$, $std \in [0.165, 0.236]$), indicating that a sparse subset of metrics captures the mergeability signal more reliably. Importantly, L_1 regularization consistently eliminates effective-rank metrics, while subspace and gradient-based metrics are selected with near-100% frequency across folds (Figure 5). This confirms that the identified stable predictors are not artifacts of coefficient scaling or redundancy, but reflect robust, method-independent signals of mergeability. We therefore present the dense (unregularized) model in the main analysis to expose relative contributions across the full metric set, enabling direct comparison of method-specific fingerprints, while using L_1 regularization as a robustness check.

7.2. Metric Category Ablation

To validate the coefficient-based analysis, we perform ablation experiments by removing entire metric categories from the linear optimization. Consistent with the learned coefficients, subspace and gradient-based metrics prove most influential: removing subspace overlap results in the largest performance degradation (average $\Delta r = -0.123$), while excluding gradient-based metrics also leads to a sub-

stantial drop (average $\Delta r = -0.064$). These results mirror the stable-metric analysis, where right subspace overlap and gradient L_2 distance exhibited the most consistent and high-magnitude coefficients.

Notably, SVD-based methods (TSV and Isotropic) are most sensitive to the removal of subspace metrics, reflecting their reliance on low-rank structures within shared representation subspaces. Conversely, categories such as effective-rank metrics contribute marginally ($\Delta r \leq -0.01$). This outcome demonstrates the framework’s ability to isolate dominant signals and identify redundancy without prior knowledge. Furthermore, metrics that appear redundant here may prove informative for future merging algorithms based on different optimization principles (see Appendix A.7).

8. Limitations

Although our framework is method- and architecture-agnostic, our evaluation solely focuses on CLIP ViT-B/16; distinct geometric behaviors may emerge in other architectures or modalities. Furthermore, while our 20-task benchmark (Gargiulo et al., 2024) is the largest of its kind, the resulting 190 task pairs may not fully capture the full diversity of the domain. Some pairwise metrics also require calibration data, limiting their utility in extremely data-scarce settings. Additionally, we focus on pairwise merging, whereas merging multiple models may introduce higher-order interference. Finally, while we prioritize interpretability through a linear model, we acknowledge that more complex non-linear interactions between metrics might exist, though our current data scale favors the robustness of a linear approach.

9. Conclusion

In this work, we move beyond the concept of intrinsic mergeability, showing that success is governed by pairwise model properties and specific merging mechanics. Using an interpretable linear framework as a diagnostic probe, we show that each merging method exhibits a distinct “success fingerprint” by prioritizing different, and often conflicting, characteristics. This variability confirms that mergeability is a method-dependent navigation of weight and functional landscapes rather than a fixed scalar attribute.

Beyond explanation, our framework yields testable predictions: LOTO evaluation confirms generalization to unseen tasks, while low metric overlap across algorithms reveals method-dependent compatibility. Simultaneously, stable metrics identify method-agnostic signals, specifically gradient distance and dominant subspace overlap. These findings provide both diagnostic tools for understanding merging failures and a roadmap for transitioning from heuristic-based merging toward principled, merge-aware fine-tuning and models that are compatible by construction.

Acknowledgements

This work is supported by the MUR FIS2 grant n. FIS-2023-00942 "NEXUS" (cup B53C25001030001), and partly by Sapienza University of Rome via the Seed of ERC grant "MINT.AI" (cup B83C25001040001).

Broader Impact Statement

This paper presents work whose goal is to advance the field of Machine Learning by providing an interpretable framework for predicting the success of model merging. By identifying specific pairwise properties, such as gradient distance and subspace overlap, that determine mergeability, our research enables practitioners to combine task-specific models more reliably without the need for expensive joint retraining.

From a societal and ethical perspective, this work contributes to more sustainable AI development by reducing the computational resources and energy consumption required to create multi-task systems. Furthermore, by moving away from black-box predictors toward a transparent, linear model of mergeability, we enhance the interpretability of model interactions. This transparency is a critical step toward understanding and mitigating potential failures or performance degradations in merged models used in downstream applications.

LLM Usage Statement

The authors leveraged LLMs to assist in the following tasks:

- **Polishing the paper:** Refining the language for clarity, correcting grammatical errors, and ensuring stylistic consistency throughout the manuscript.
- **Assisting in code writing:** Aiding in the development and debugging of the scripts used for the experimental evaluation of model mergeability.
- **Writing code to generate LaTeX tables:** Automating the conversion of raw experimental data into LaTeX table syntax and refining complex formatting, such as multi-row alignment and column spacing.

References

Bolton, O., Aakanksha, Ahmadian, A., Hooker, S., Fadaee, M., and Ermis, B. Simmerge: Learning to select merge operators from similarity signals, 2026. URL <https://arxiv.org/abs/2601.09473>.

Bossard, L., Guillaumin, M., and Van Gool, L. Food-101 – Mining Discriminative Components with Random Forests. In Fleet, D., Pajdla, T., Schiele, B., and Tuytelaars, T. (eds.), *Computer Vision – ECCV 2014*, pp. 446–461, Cham, 2014. Springer International Publishing. ISBN 978-3-319-10599-4. doi: 10.1007/978-3-319-10599-4_29.

Cheng, G., Han, J., and Lu, X. Remote Sensing Image Scene Classification: Benchmark and State of the Art. *Proceedings of the IEEE*, 105(10):1865–1883, October 2017. ISSN 1558-2256. doi: 10.1109/JPROC.2017.2675998. URL <https://ieeexplore.ieee.org/document/7891544/?arnumber=7891544>. Conference Name: Proceedings of the IEEE.

Cimpoi, M., Maji, S., Kokkinos, I., Mohamed, S., and Vedaldi, A. Describing Textures in the Wild. In *2014 IEEE Conference on Computer Vision and Pattern Recognition*, pp. 3606–3613, Columbus, OH, USA, June 2014. IEEE. ISBN 978-1-4799-5118-5. doi: 10.1109/CVPR.2014.461. URL <https://ieeexplore.ieee.org/document/6909856>.

Clanuwat, T., Bober-Irizar, M., Kitamoto, A., Lamb, A., Yamamoto, K., and Ha, D. Deep Learning for Classical Japanese Literature, November 2018. URL <http://arxiv.org/abs/1812.01718>. arXiv:1812.01718 [cs, stat].

Coates, A., Ng, A., and Lee, H. An Analysis of Single-Layer Networks in Unsupervised Feature Learning. In *Proceedings of the Fourteenth International Conference on Artificial Intelligence and Statistics*, pp. 215–223. JMLR Workshop and Conference Proceedings, June 2011. URL <https://proceedings.mlr.press/v15/coates11a.html>. ISSN: 1938-7228.

Cohen, G., Afshar, S., Tapson, J., and van Schaik, A. EMNIST: Extending MNIST to handwritten letters. In *2017 International Joint Conference on Neural Networks (IJCNN)*, pp. 2921–2926, May 2017. doi: 10.1109/IJCNN.2017.7966217. URL <https://ieeexplore.ieee.org/document/7966217/?arnumber=7966217>. ISSN: 2161-4407.

Crisostomi, D., Fumero, M., Baieri, D., Bernard, F., and Rodolà, E. c^2m^3 : Cycle-consistent multi-model merging. In *Advances in Neural Information Processing Systems*, volume 37, 2024.

Daheim, N., Möllenhoff, T., Ponti, E., Gurevych, I., and Khan, M. E. Model merging by uncertainty-based gradient matching. In *The Twelfth International Conference on Learning Representations*, 2024. URL <https://openreview.net/forum?id=D7KJmfEDQP>.

Davari, M. and Belilovsky, E. Model breadcrumbs: Scaling multi-task model merging with sparse masks. *ArXiv preprint*, abs/2312.06795, 2023. URL <https://arxiv.org/abs/2312.06795>.

Deep, P. T., Bhardwaj, R., and Poria, S. Della-merging: Reducing interference in model merging through magnitude-based sampling. *CoRR*, 2024.

Frankle, J., Dziugaite, G. K., Roy, D., and Carbin, M. Linear mode connectivity and the lottery ticket hypothesis. In *Proceedings of the 37th International Conference on Machine Learning, ICML 2020, 13-18 July 2020, Virtual Event*, volume 119 of *Proceedings of Machine Learning Research*. PMLR, 2020. URL <http://proceedings.mlr.press/v119/frankle20a.html>.

Gargiulo, A. A., Crisostomi, D., Bucarelli, M. S., Scardapane, S., Silvestri, F., and Rodolà, E. Task singular vectors: Reducing task interference in model merging. *arXiv preprint arXiv:2412.00081*, 2024.

Goodfellow, I. J., Erhan, D., Carrier, P. L., Courville, A., Mirza, M., Hamner, B., Cukierski, W., Tang, Y., Thaler, D., Lee, D.-H., Zhou, Y., Ramaiah, C., Feng, F., Li, R., Wang, X., Athanasakis, D., Shawe-Taylor, J., Miliakov, M., Park, J., Ionescu, R., Popescu, M., Grozea, C., Bergstra, J., Xie, J., Romaszko, L., Xu, B., Chuang, Z., and Bengio, Y. Challenges in Representation Learning: A Report on Three Machine Learning Contests. In Lee, M., Hirose, A., Hou, Z.-G., and Kil, R. M. (eds.), *Neural Information Processing*, pp. 117–124, Berlin, Heidelberg, 2013. Springer. ISBN 978-3-642-42051-1. doi: 10.1007/978-3-642-42051-1_16.

Helber, P., Bischke, B., Dengel, A., and Borth, D. EuroSAT: A Novel Dataset and Deep Learning Benchmark for Land Use and Land Cover Classification. *IEEE Journal of Selected Topics in Applied Earth Observations and Remote Sensing*, 12(7):2217–2226, July 2019. ISSN 2151-1535. doi: 10.1109/JSTARS.2019.2918242. URL <https://ieeexplore.ieee.org/document/8736785/?arnumber=8736785>. Conference Name: IEEE Journal of Selected Topics in Applied Earth Observations and Remote Sensing.

Ilharco, G., Ribeiro, M. T., Wortsman, M., Gururangan, S., Schmidt, L., Hajishirzi, H., and Farhadi, A. Editing models with task arithmetic. In *International Conference on Learning Representations*, 2023.

Kingma, D. P. and Ba, J. Adam: A method for stochastic optimization. *arXiv preprint arXiv:1412.6980*, 2014.

Krause, J., Stark, M., Deng, J., and Fei-Fei, L. 3d object representations for fine-grained categorization. In *Proceedings of the IEEE international conference on computer vision workshops*, pp. 554–561, 2013.

Krizhevsky, A. and Hinton, G. Learning multiple layers of features from tiny images. Technical Report 0, University of Toronto, Toronto, Ontario, 2009. URL <https://www.cs.toronto.edu/~kriz/learning-features-2009-TR.pdf>.

Lecun, Y., Bottou, L., Bengio, Y., and Haffner, P. Gradient-based learning applied to document recognition. *Proceedings of the IEEE*, 86(11):2278–2324, 1998. doi: 10.1109/5.726791.

Li, W., Peng, Y., Zhang, M., Ding, L., Hu, H., and Shen, L. Deep model fusion: A survey. *arXiv preprint arXiv:2309.15698*, 2023.

Liu, Z., Wu, H., Yao, Y., She, R., Han, X., Zhong, T., and Yuan, M. Lore-merging: Exploring low-rank estimation for large language model merging. *arXiv preprint arXiv:2502.10749*, 2025.

Marczak, D., Magistri, S., Cygert, S., Twardowski, B., Bagdanov, A. D., and van de Weijer, J. No task left behind: Isotropic model merging with common and task-specific subspaces. In *Forty-second International Conference on Machine Learning*.

Matena, M. S. and Raffel, C. A. Merging models with fisher-weighted averaging. *Advances in Neural Information Processing Systems*, 35:17703–17716, 2022.

Netzer, Y., Wang, T., Coates, A., Bissacco, A., Wu, B., and Ng, A. Y. Reading digits in natural images with unsupervised feature learning. In *NIPS Workshop on Deep Learning and Unsupervised Feature Learning 2011*, 2011. URL http://ufldl.stanford.edu/housenumbers/nips2011_housenumbers.pdf.

Nilsback, M.-E. and Zisserman, A. Automated Flower Classification over a Large Number of Classes. In *2008 Sixth Indian Conference on Computer Vision, Graphics & Image Processing*, pp. 722–729, December 2008. doi: 10.1109/ICVGIP.2008.47. URL <https://ieeexplore.ieee.org/document/4756141>.

Ortiz-Jimenez, G., Favero, A., and Frossard, P. Task arithmetic in the tangent space: Improved editing of pre-trained models. *Advances in Neural Information Processing Systems*, 2024.

Parkhi, O. M., Vedaldi, A., Zisserman, A., and Jawahar, C. V. Cats and dogs. In *2012 IEEE Conference on Computer Vision and Pattern Recognition*, pp. 3498–3505, June 2012. doi: 10.1109/CVPR.2012.6248092. URL <https://ieeexplore.ieee.org/document/6248092>. ISSN: 1063-6919.

Radford, A., Kim, J. W., Hallacy, C., Ramesh, A., Goh, G., Agarwal, S., Sastry, G., Askell, A., Mishkin, P., Clark, J., et al. Learning transferable visual models from natural

language supervision. In *International Conference on Machine Learning*, 2021.

Rahamim, A., Yehudai, A., Carmeli, B., Choshen, L., Mass, Y., and Belinkov, Y. Will it merge? on the causes of model mergeability, 2026. URL <https://arxiv.org/abs/2601.06672>.

Socher, R., Perelygin, A., Wu, J., Chuang, J., Manning, C. D., Ng, A., and Potts, C. Recursive deep models for semantic compositionality over a sentiment treebank. In Yarowsky, D., Baldwin, T., Korhonen, A., Livescu, K., and Bethard, S. (eds.), *Proceedings of the 2013 Conference on Empirical Methods in Natural Language Processing*, pp. 1631–1642, Seattle, Washington, USA, October 2013. Association for Computational Linguistics. URL <https://aclanthology.org/D13-1170>.

Stallkamp, J., Schlipsing, M., Salmen, J., and Igel, C. The German Traffic Sign Recognition Benchmark: A multi-class classification competition. In *The 2011 International Joint Conference on Neural Networks*, pp. 1453–1460, July 2011. doi: 10.1109/IJCNN.2011.6033395. URL <https://ieeexplore.ieee.org/document/6033395/?arnumber=6033395>. ISSN: 2161-4407.

Veeling, B. S., Linmans, J., Winkens, J., Cohen, T., and Welling, M. Rotation Equivariant CNNs for Digital Pathology. In Frangi, A. F., Schnabel, J. A., Davatzikos, C., Alberola-López, C., and Fichtinger, G. (eds.), *Medical Image Computing and Computer Assisted Intervention – MICCAI 2018*, pp. 210–218, Cham, 2018. Springer International Publishing. ISBN 978-3-030-00934-2. doi: 10.1007/978-3-030-00934-2_24.

Wang, K., Dimitriadis, N., Ortiz-Jiménez, G., Fleuret, F., and Frossard, P. Localizing task information for improved model merging and compression. In *Proceedings of the 41st International Conference on Machine Learning*, pp. 50268–50287, 2024a.

Wang, K., Dimitriadis, N., Ortiz-Jimenez, G., Fleuret, F., and Frossard, P. Localizing task information for improved model merging and compression. In *Forty-first International Conference on Machine Learning*, 2024b.

Wortsman, M., Ilharco, G., Gadre, S. Y., Roelofs, R., Gontijo-Lopes, R., Morcos, A. S., Namkoong, H., Farhadi, A., Carber, Y., Kornblith, S., et al. Model soups: averaging weights of multiple fine-tuned models improves accuracy without increasing inference time. In *International Conference on Machine Learning*, 2022.

Xiao, H., Rasul, K., and Vollgraf, R. Fashion-MNIST: a Novel Image Dataset for Benchmarking Machine Learning Algorithms, September 2017. URL <http://arxiv.org/abs/1708.07747>. arXiv:1708.07747 [cs, stat].

Xiao, J., Ehinger, K. A., Hays, J., Torralba, A., and Oliva, A. SUN Database: Exploring a Large Collection of Scene Categories. *International Journal of Computer Vision*, 119(1):3–22, August 2016. ISSN 1573-1405. doi: 10.1007/s11263-014-0748-y. URL <https://doi.org/10.1007/s11263-014-0748-y>.

Yadav, P., Tam, D., Choshen, L., Raffel, C., and Bansal, M. Ties-merging: Resolving interference when merging models. 2023.

Yang, E., Wang, Z., Shen, L., Liu, S., Guo, G., Wang, X., and Tao, D. Adamerging: Adaptive model merging for multi-task learning. In *The Twelfth International Conference on Learning Representations*, 2023.

Yang, E., Shen, L., Wang, Z., Guo, G., Chen, X., Wang, X., and Tao, D. Representation surgery for multi-task model merging. *ArXiv preprint*, abs/2402.02705, 2024. URL <https://arxiv.org/abs/2402.02705>.

Yu, T., Kumar, S., Gupta, A., Levine, S., Hausman, K., and Finn, C. Gradient surgery for multi-task learning. In *Advances in Neural Information Processing Systems*, 2020.

Zhou, L., Solombrino, D., Crisostomi, D., Bucarelli, M. S., D’Inverno, G. A., Silvestri, F., and Rodolà, E. On task vectors and gradients. *arXiv preprint arXiv:2508.16082*, 2025a.

Zhou, L., Solombrino, D., Crisostomi, D., Bucarelli, M. S., Silvestri, F., and Rodolà, E. Atm: Improving model merging by alternating tuning and merging, 2025b. URL <https://arxiv.org/abs/2411.03055>.

A. Appendix

A.1. Individual Metric Correlations

To motivate the need for a learned linear combination of mergeability metrics, we examine the predictive power of each metric in isolation. Table 5 reports the Pearson correlation between each individual metric and the normalized post-merge accuracy (i.e., post-merge performance divided by task-specific model performance, averaged across the two tasks) across all 190 task pairs, computed separately for each merging method.

The results reveal that no single metric consistently achieves strong correlations across all merging methods. The highest individual correlations are observed for activation-based metrics, particularly activation dot product ($r = 0.572$ for TSV, $r = 0.450$ for Weight Averaging) and activation cosine similarity ($r = 0.521$ for TSV, $r = 0.366$ for Weight Averaging). However, these same metrics show weak or non-significant correlations for Task Arithmetic ($r = 0.094$, $r = 0.146$) and Isotropic merging ($r = -0.095$, $r = 0.062$), indicating that their predictive utility is method-dependent.

Task vector geometry metrics, which are computationally inexpensive and have been proposed as indicators of mergeability in prior work, show uniformly weak correlations (typically $|r| < 0.1$) across all methods. Similarly, effective rank metrics achieve at most weak correlations ($|r| < 0.2$), despite theoretical motivation linking spectral properties to merge success.

Subspace overlap metrics exhibit an interesting pattern: metrics focusing on bottom singular vectors (Right Sub Bot- k , Interact Bot- k) show moderate correlations for Task Arithmetic ($r \approx 0.21$) and Isotropic merging ($r \approx 0.31$), but near-zero correlations for Weight Averaging and TSV. This suggests that different aspects of task vector geometry are relevant for different merging strategies.

The inconsistency of individual metric correlations across methods underscores a key finding: mergeability prediction requires combining multiple complementary signals. A metric that is predictive for one method may be uninformative or even misleading for another. This observation motivates our approach of learning method-specific weighted combinations of metrics, which achieves substantially higher correlations (see Section 6) by leveraging the complementary information captured by different metric categories.

A.2. MLP Ablation Study

To investigate whether non-linear combinations of mergeability metrics could yield superior predictive performance compared to our linear approach, we conducted an ablation study using Multi-Layer Perceptrons (MLPs). For each merging method, we trained separate MLPs to predict post-merge performance from the same 28 mergeability metrics used in the linear model.

Experimental Setup. Each MLP consists of a single hidden layer with 8 units, ReLU activation, and dropout regularization (rate 0.4), resulting in 249 trainable parameters per model. We use the same leave-one-task-out (LOTO) cross-validation protocol as the linear model: for each of the 20 tasks, we train on pairs from the remaining 19 tasks and evaluate on pairs involving the held-out task. This results in 20 separate model trainings per merging method, with predictions aggregated across all folds. Models were trained for 300 epochs using the Adam optimizer with a learning rate of 0.001, optimizing mean squared error loss.

Results. Table 6 compares the validation Pearson correlations achieved by the MLP models against the linear combination approach under identical LOTO cross-validation settings.

The results show that the MLP models generally underperform the simpler linear approach, while also exhibiting generally higher variance across the validation folds:

- **Task Arithmetic:** The MLP shows substantial degradation, achieving only $r = 0.084$ compared to $r = 0.343$ for the linear model. This suggests the MLP overfits to spurious patterns in the training data that do not generalize across tasks.
- **Weight Averaging:** The MLP achieves $r = 0.407$, lower than the linear model's $r = 0.555$, with considerably higher variance across folds ($\text{std} = 0.308$ vs 0.165).
- **Isotropic:** This is the only case the MLPs show improvement ($r = 0.426$ vs. $r = 0.328$), though the difference is within one standard deviation.
- **TSV:** Both approaches achieve similar performance ($r = 0.572$ vs. $r = 0.570$), with the MLP showing higher variance

Table 5. Pearson correlation between individual mergeability metrics and normalized post-merge accuracy. Cell shading indicates significance levels (Darkest: $p < 0.001$, Medium: $p < 0.01$, Lightest: $p < 0.05$), with no share signifying statistical insignificance.

Metric	Task Arithmetic	Weight Averaging	Isotropic	TSV
Task Vector	Task Vector Cosine Sim	0.015	0.030	-0.043
	Task Vector L_2 Dist	-0.079	-0.079	-0.041
	Task Vector Dot Prod	-0.015	0.020	-0.073
	Weight Angle	-0.017	-0.032	0.041
	Task Vector Mag Ratio	-0.037	0.057	-0.094
Effective Rank	Eff Rank	-0.009	0.116	-0.064
	Eff Rank Score	0.009	-0.116	0.064
	Stable Rank	-0.014	0.104	-0.068
	Spectral Gap	0.032	-0.065	0.084
	SV Ratio	-0.032	0.065	-0.084
	Layer Eff Rank	0.015	0.136	-0.044
	Layer Eff Rank Score	-0.015	-0.136	0.044
Sub. Overlap	SV Overlap	-0.167	-0.164	-0.150
	Left Sub Top- k	0.093	-0.007	0.073
	Right Sub Top- k	0.062	-0.051	0.060
	Right Sub Bot- k	0.211	0.009	0.319
	Interact Top- k	0.071	0.006	0.040
	Interact Bot- k	0.209	0.006	0.312
Activation	Act L_2 Dist	-0.167	-0.313	-0.121
	Act Cosine Sim	0.146	0.366	0.062
	Act Mag Ratio	0.050	-0.001	0.062
	Act Dot Prod	0.094	0.450	-0.095
Gradient	Enc Grad Cos	0.012	0.086	-0.014
	Enc Grad L_2	-0.099	-0.257	0.027
	Enc Grad Dot	0.061	0.082	0.037
	Input Grad Cos	-0.035	-0.020	0.008
	Input Grad L_2	-0.162	-0.322	-0.032
	Input Grad Dot	-0.067	-0.083	-0.040

Table 6. Comparison of validation Pearson correlation (r) between linear combination and MLP approaches for predicting post-merge performance using leave-one-task-out cross-validation. Despite greater model capacity (249 vs. 28 parameters), MLPs do not consistently improve upon the linear baseline and show higher variance across folds.

Method	Linear (Val r)	Linear (Val r std)	MLP (Val r)	MLP (Val r std)	Δ_r
Task Arithmetic	0.343	0.25	0.084	0.227	-0.259
Weight Averaging	0.555	0.165	0.407	0.308	-0.148
Isotropic	0.328	0.227	0.426	0.178	+0.098
TSV	0.572	0.236	0.570	0.328	-0.002

(std = 0.328 vs 0.236).

Why Do MLPs Underperform? Although MLPs are theoretically more expressive than linear models, several factors explain their inferior performance in this setting:

1. **Limited training data:** With only approximately 190 task pairs total and approximately 160 training pairs per fold, the dataset is too small to reliably learn non-linear relationships. The MLP’s 249 parameters (versus 28 for the linear model) create a high parameter-to-sample ratio that promotes overfitting. Classical statistical theory suggests that reliable estimation requires at least 10–20 samples per parameter; our setting provides fewer than 1 sample per MLP parameter.
2. **High-dimensional input space:** With 28 input metrics, the MLP must learn meaningful interactions in a 28-dimensional space from limited samples. The curse of dimensionality makes it exponentially harder to identify true non-linear patterns versus spurious correlations as dimensionality increases.
3. **Task distribution shift:** The LOTO evaluation requires generalization to entirely new tasks. Non-linear models can memorize task-specific patterns that appear useful on training tasks but fail catastrophically on held-out tasks. Linear models, being more constrained, are forced to learn simpler relationships that transfer better.
4. **Noise amplification:** If the underlying relationship is approximately linear with noise, an MLP will attempt to fit the noise through non-linear transformations, leading to worse generalization. The linear model’s inductive bias acts as implicit regularization.

Discussion. These results support our choice of a linear combination approach for several reasons:

1. **Interpretability:** Linear coefficients directly indicate the relative importance and direction of each metric’s contribution, facilitating analysis of which pairwise mergeability metrics matter for each merging method. This transparency is crucial for understanding *why* certain task pairs are predicted to merge well or poorly.
2. **Robustness:** The linear model shows more consistent generalization across all merging methods, whereas MLPs exhibit high variance across folds and degrade substantially for some methods.
3. **Appropriate inductive bias:** Given the limited data and the need to generalize across diverse tasks, the linear model’s simplicity is a feature rather than a limitation. It captures the dominant signal without overfitting to noise.

The failure of MLPs to improve upon linear combinations suggests that the relationship between mergeability metrics and post-merge performance is approximately linear, or at least that any non-linear patterns are too subtle to reliably capture with the available data. This finding aligns with similar observations in other domains where simpler models outperform complex ones when data is scarce relative to model capacity.

A.3. Learned Coefficient Values

While the main paper discusses the learned coefficients for all methods, here we provide a visual representation of these coefficients through a heatmap (4) and the exact numerical coefficients in Table 9. These coefficients are obtained by averaging across all 20 folds of the leave-one-task-out cross-validation procedure, for each merging method. The coefficients operate on min-max normalized metrics (scaled to $[-1, 1]$), with normalization statistics computed only on training data within each fold to prevent data leakage.

Interpretation. A positive coefficient indicates that higher values of the corresponding metric predict better post-merge performance, while a negative coefficient indicates the opposite relationship. The magnitude of a coefficient reflects how strongly that metric influences the prediction, though direct comparison across metrics requires accounting for their different variances.

Dominant Metric Overlap. We examine the overlap between top-5 and top-10 most dominant metrics (by average magnitude coefficient) across methods. Two methods exhibit an overlap of 1.0 when their top- k metrics are completely the same set. Tables 7 and 8 illustrate these overlaps. We observe that overlap is generally small, especially for the top-5 metrics, ranging from 0.2 between WA and TSV to a 0.6 in three occasions. For the top-10 metrics, figures are similar, with increased overlap due to the expanded set of metrics. Interestingly, the best overlapping method pairs remain consistent, i.e., TA-ISO, WA-ISO, and TA-TSV. Likewise, the least overlapping pair, WA-TSV, also remains consistent in both scenarios.

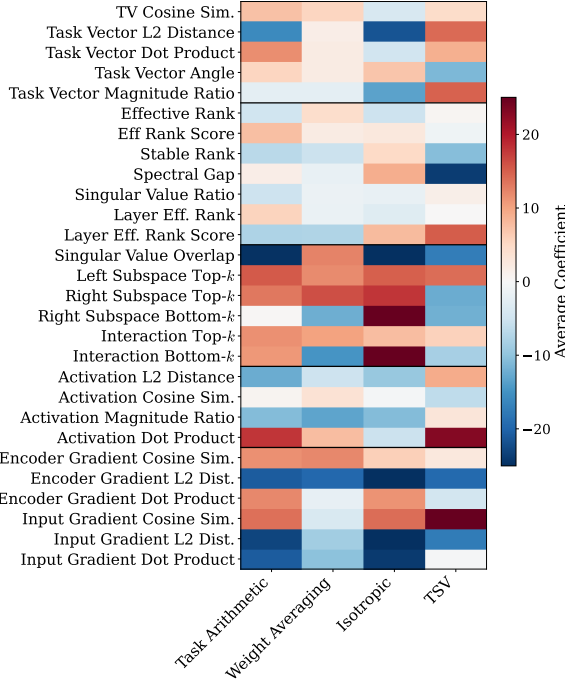


Figure 4. Per-method learned coefficients for all 28 metrics, averaged across the 20 leave-one-task-out folds.

This demonstrates that metric overlap is not sensitive to the noise in the top-5 metrics but showcases the actual dissimilarities in factors determining mergeability for different methods.

Table 7. Overlap of top-5 metrics among methods. Average cross-method overlap is 0.47.

Method	TA	WA	ISO	TSV
TA	1.0	0.4	0.6	0.6
WA		1.0	0.6	0.2
ISO			1.0	0.4
TSV				1.0

Table 8. Overlap of top-10 metrics among methods. Average cross-method overlap is 0.6.

Method	TA	WA	ISO	TSV
TA	1.0	0.5	0.8	0.7
WA		1.0	0.7	0.3
ISO			1.0	0.6
TSV				1.0

Sign Agreement. In Table 10, we report the percentage of agreement in coefficient signs across the 28 metrics for each pair of methods. An agreement of 1.0 indicates that the two methods share the same average coefficient sign for all metrics, whereas 0% denotes complete sign opposition. Overall, the results reveal substantial sign disagreement between methods, particularly in comparisons involving TSV, where most metrics exhibit opposing coefficient signs.

Stable Metrics. Six metrics exhibit a consistent sign across all four merging methods, suggesting they capture fundamental aspects of mergeability:

- **Negative coefficients (higher values predict worse merging):**
 - Encoder gradient L_2 distance (avg: -23.3, range: [-33.3, -19.5])

- Input gradient L_2 distance (avg: -21.4 , range: $[-36.3, -8.7]$)
- Input gradient dot product (avg: -13.9 , range: $[-24.0, -0.2]$)
- **Positive coefficients (higher values predict better merging):**
 - Left subspace overlap top- k (avg: $+14.0$, range: $[+11.8, +15.4]$)
 - Interaction matrix overlap top- k (avg: $+8.8$, range: $[+5.8, +11.5]$)
 - Encoder gradient cosine similarity (avg: $+8.1$, range: $[+2.7, +12.1]$)

Key Observations. Several patterns emerge from the coefficient values:

- **Gradient-based metrics** consistently receive large-magnitude coefficients. The L_2 distance metrics for both encoder and input gradients show negative coefficients across all methods, indicating that large gradient differences between task vectors are detrimental to merging success.
- **Subspace overlap metrics** tend to receive positive coefficients, suggesting that task vectors sharing similar principal directions merge more effectively.
- **Method-specific patterns:** Different merging methods exhibit drastically different coefficients across the metrics, and no obvious pattern emerges.
- **High variance:** Many coefficients exhibit high standard deviation across folds (often exceeding the mean), reflecting the challenge of learning stable predictors from limited data and the sensitivity to which task is held out.

Table 10. Coefficient sign agreement between methods. Average cross-method agreement is 0.55.

Method	TA	WA	ISO	TSV
TA	1.0	0.68	0.75	0.46
WA		1.0	0.50	0.57
ISO			1.0	0.36
TSV				1.0

A.4. Mergeability Metrics: Definitions and Implementation Details

This appendix provides formal definitions and implementation details for the mergeability metrics summarized in Section 3 of the main paper.

We introduce a suite of 28 pairwise metrics to study model compatibility. Since no single metric is sufficiently predictive (A.1), we leverage their combined expressivity to characterize mergeability. These metrics are computed without performing the merge, enabling efficient pre-screening of model pairs. For layer-wise metrics, we report the mean across all layers. We categorize these metrics into five distinct groups, detailed below.

A.4.1. TASK VECTOR GEOMETRY METRICS

Given two task vectors $\tau_A, \tau_B \in \mathbb{R}^D$, defined as the flattened 1D differences $\theta_i - \theta_0$ between finetuned and pretrained weights, the most direct approach to measuring compatibility examines their geometric relationship in weight space. The intuition is that task vectors pointing in similar directions may interfere less during merging.

- **Cosine Similarity:** Measures directional alignment between task vectors: $\frac{\tau_A \cdot \tau_B}{\|\tau_A\|_2 \|\tau_B\|_2}$.
- **L_2 Distance:** Euclidean distance between task vectors: $\|\tau_A - \tau_B\|_2$. Small distances indicate similar updates.
- **Dot Product:** Captures both direction and magnitude: $\tau_A \cdot \tau_B$. This potentially identifies cases where one task dominates the weight space.
- **Weight Space Angle:** The angle $\theta = \arccos(\cos \text{ sim})$ in degrees, providing an interpretable measure of directional difference.
- **Magnitude Ratio:** Expressed as the ratio between the two task vector magnitudes: $\min(\|\tau_A\|, \|\tau_B\|) / \max(\|\tau_A\|, \|\tau_B\|)$. A ratio close to 1 suggests balanced contributions from both tasks

Table 9. Average learned coefficients (\pm standard deviation) for each mergeability metric across merging methods, obtained via leave-one-task-out cross-validation. Positive coefficients indicate that higher metric values predict better post-merge performance, while negative coefficients indicate the opposite. Coefficients are on normalized metrics (min-max scaled to $[-1, 1]$).

	Metric	Task Arithmetic	Weight Averaging	Isotropic	TSV
Task Vector	TV Cosine Sim	7.29 \pm 13.52	5.30 \pm 23.63	-3.94 \pm 21.35	4.67 \pm 16.87
	TV L_2 Dist	-15.87 \pm 28.31	1.64 \pm 19.68	-21.65 \pm 25.83	14.24 \pm 67.77
	TV Dot Prod	11.64 \pm 18.54	2.02 \pm 8.33	-4.70 \pm 35.30	9.04 \pm 49.82
	Weight Angle	5.38 \pm 22.34	1.97 \pm 12.85	6.96 \pm 35.91	-11.26 \pm 42.49
	TV Mag Ratio	-2.43 \pm 20.99	-2.42 \pm 20.67	-13.42 \pm 31.20	14.74 \pm 59.51
Effective Rank	Eff Rank	-4.89 \pm 21.27	4.42 \pm 16.66	-5.16 \pm 22.16	0.50 \pm 8.72
	Eff Rank Score	7.52 \pm 31.63	1.99 \pm 9.13	2.60 \pm 29.13	-1.11 \pm 6.38
	Stable Rank	-6.66 \pm 23.98	-5.54 \pm 18.40	5.08 \pm 24.20	-10.85 \pm 60.41
	Spectral Gap	1.56 \pm 23.22	-1.93 \pm 10.03	9.19 \pm 22.79	-23.82 \pm 97.44
	SV Ratio	-5.24 \pm 16.14	-1.42 \pm 7.45	-1.76 \pm 27.51	1.61 \pm 17.74
	Layer Eff Rank	5.63 \pm 11.35	-1.69 \pm 13.82	-3.04 \pm 28.06	-0.04 \pm 34.31
	Layer Eff Rank Score	-7.68 \pm 17.89	-7.52 \pm 41.90	7.96 \pm 31.07	15.13 \pm 55.60
Sub. Overlap	SV Overlap	-24.72 \pm 30.35	12.51 \pm 50.12	-27.10 \pm 33.94	-17.28 \pm 84.90
	Left Sub Top- k	15.36 \pm 24.81	11.78 \pm 37.52	15.01 \pm 19.12	13.97 \pm 41.16
	Right Sub Top- k	13.30 \pm 27.66	16.22 \pm 45.82	17.94 \pm 39.59	-12.44 \pm 85.74
	Right Sub Bot- k	0.38 \pm 19.05	-12.27 \pm 24.81	35.02 \pm 37.43	-11.88 \pm 40.54
	Interact Top- k	11.48 \pm 19.11	10.10 \pm 20.77	7.69 \pm 21.26	5.84 \pm 10.85
	Interact Bot- k	10.99 \pm 25.62	-14.78 \pm 41.54	30.28 \pm 32.48	-8.32 \pm 15.88
Activation	Act L_2 Dist	-12.40 \pm 15.51	-5.33 \pm 23.35	-9.56 \pm 22.16	9.23 \pm 45.68
	Act Cosine Sim	0.70 \pm 14.38	3.58 \pm 16.79	-0.46 \pm 23.20	-6.44 \pm 57.81
	Act Mag Ratio	-10.79 \pm 12.31	-13.26 \pm 43.32	-10.84 \pm 26.74	2.99 \pm 31.21
	Act Dot Prod	17.93 \pm 32.81	7.83 \pm 13.00	-5.49 \pm 34.66	22.96 \pm 57.75
Gradient	Enc Grad Cos	11.41 \pm 17.38	12.08 \pm 28.82	5.99 \pm 19.84	2.70 \pm 6.59
	Enc Grad L_2	-20.84 \pm 24.07	-19.64 \pm 33.51	-33.31 \pm 36.45	-19.53 \pm 31.77
	Enc Grad Dot	12.00 \pm 19.98	-2.11 \pm 33.79	11.17 \pm 14.96	-4.63 \pm 28.26
	Input Grad Cos	13.86 \pm 27.17	-3.87 \pm 43.09	13.96 \pm 27.54	25.42 \pm 97.25
	Input Grad L_2	-23.00 \pm 27.05	-8.72 \pm 19.82	-36.30 \pm 39.11	-17.59 \pm 45.52
	Input Grad Dot	-20.90 \pm 26.55	-10.32 \pm 21.91	-24.03 \pm 41.71	-0.25 \pm 33.86

Table 11. Summary of mergeability metrics by category.

Category	Metrics	Count
Task Vector	cos sim, L_2 dist., dot, angle, magnitude ratio	5
Effective Rank	eff rank, stable rank, spectral gap, etc.	7
Subspace Overlap	SV overlap, subspace overlap, interaction	6
Activation-Based	L_2 dist., cosine sim., magnitude ratio, dot	4
Gradient-Based	encoder/input grad. L_2 dist., cos sim, dot	6
Total		28

A.4.2. EFFECTIVE RANK METRICS

Recent work shows task arithmetic benefits from low-rank task vectors (Liu et al., 2025). We propose metrics based on the *effective rank* of task vectors to capture this property.

Given the $2 \times D$ matrix $\mathbf{T} = [\boldsymbol{\tau}_A; \boldsymbol{\tau}_B]^\top$ formed by stacking the two task vectors, we compute its singular value decomposition to obtain singular values $\sigma_1 \geq \sigma_2$.

- **Effective Rank:** The participation ratio based on singular value entropy:

$$\text{EffRank}(\mathbf{T}) = \exp \left(- \sum_i p_i \log p_i \right), \quad p_i = \frac{\sigma_i}{\sum_j \sigma_j} \quad (4)$$

An effective rank of 1 indicates a perfect low-rank structure (all mass in one direction), while higher values indicate more diffuse subspaces.

- **Effective Rank Mergeability Score:** A normalized version mapping effective rank from $[1, 2]$ to $[1, 0]$, where higher scores indicate better compatibility.
- **Stable Rank:** An alternative dimensionality measure using the squared Frobenius norm:

$$\text{StableRank}(\mathbf{T}) = \frac{(\sum_i \sigma_i)^2}{\sum_i \sigma_i^2} \quad (5)$$

- **Spectral Gap:** The normalized difference between singular values $(\sigma_1 - \sigma_2)/\sigma_1$. A large gap indicates one dominant direction, suggesting alignment.
- **Singular Value Ratio:** The ratio σ_2/σ_1 . Smaller values indicate stronger alignment.
- **Layer-wise Effective Rank:** Computes effective rank per layer and averages, weighted by layer update magnitude $\|\boldsymbol{\tau}_A^{(\ell)}\| + \|\boldsymbol{\tau}_B^{(\ell)}\|$. This provides finer-grained insight than global effective rank.
- **Layer-wise Effective Rank Mergeability Score:** The normalized version of layer-wise effective rank.

A.4.3. SUBSPACE OVERLAP METRICS

These metrics analyze how the principal directions modified by each task vector relate to each other, based on the Singular Value Decomposition (SVD) of individual weight matrices, which decomposes a matrix $W \in \mathbb{R}^{m \times n}$ as:

$$W = U \Sigma V^\top \quad (6)$$

where $U \in \mathbb{R}^{m \times m}$ and $V \in \mathbb{R}^{n \times n}$ are orthogonal matrices containing the left and right singular vectors, and $\Sigma \in \mathbb{R}^{m \times n}$ is a diagonal matrix containing the singular values $\sigma_1 \geq \sigma_2 \geq \dots \geq 0$.

- **Singular Value Overlap:** For each 2D task vector matrix, computes the cosine similarity between the top-100 normalized singular value distributions, averaged across all layers.
- **Left Subspace Overlap:** Measures overlap between the top- k left singular vectors (columns of U) across weight matrices using the Frobenius norm of $\mathbf{U}_A^{(k)\top} \mathbf{U}_B^{(k)}$. The value of k is set to 10 here and in the following metrics.
- **Right Subspace Overlap (Top- k and Bottom- k):** Similarly measures overlap between right singular vectors (rows of V). We compute this for both the strongest (top- k) and weakest (bottom- k) singular directions, as different merging methods may be sensitive to different spectral components.

- **Interaction Matrix Overlap (Top- k and Bottom- k):** Computes the interaction matrix $\mathbf{M} = \mathbf{V}_A^{(k)\top} \mathbf{V}_B^{(k)}$ whose singular values represent cosines of principal angles between subspaces. We report the mean squared singular value of \mathbf{M} .

A.4.4. ACTIVATION-BASED METRICS

While weight-space metrics are computationally efficient, they may miss functional similarities. We complement them with activation-based metrics that measure how similarly the finetuned models process inputs.

Given a small calibration set \mathcal{D}_{cal} (10 random samples per dataset in our experiments), we extract activations from the final encoder layer of both models and compute:

- **Activation L_2 Distance:** $\|\bar{\mathbf{a}}_A - \bar{\mathbf{a}}_B\|_2$ where $\bar{\mathbf{a}}$ denotes the mean activation over calibration samples.
- **Activation Cosine Similarity:** Directional alignment of mean activations.
- **Activation Magnitude Ratio:** Ratio of activation norms, indicating whether scales are similar.
- **Activation Dot Product:** Captures both direction and magnitude of activation alignment.

A.4.5. GRADIENT-BASED METRICS

Gradient alignment has been shown to correlate with multi-task learning success (Yu et al., 2020). We leverage the same calibration set as in activation-based metrics, and measure gradient similarity at two levels:

Encoder Gradient Metrics. We compute gradients of the cross-entropy loss with respect to encoder parameters:

- **Encoder Gradient Cosine Similarity:** Measures the alignment of the directions in which models require updates: $\frac{\mathbf{g}_A \cdot \mathbf{g}_B}{\|\mathbf{g}_A\|_2 \|\mathbf{g}_B\|_2}$.
- **Encoder Gradient L_2 Distance:** Measures the Euclidean magnitude of the difference between gradient vectors: $\|\mathbf{g}_A - \mathbf{g}_B\|_2$.
- **Encoder Gradient Dot Product:** Captures both the direction and magnitude of gradient agreement: $\mathbf{g}_A \cdot \mathbf{g}_B$.

Input Gradient Metrics. We compute gradients with respect to input images to capture how models attend to them:

- **Input Gradient Cosine Similarity:** Measures whether models focus on similar input regions.
- **Input Gradient L_2 Distance:** Magnitude of input sensitivity difference.
- **Input Gradient Dot Product:** Combined direction and magnitude measure.

Table 11 summarizes all 28 metrics and their computational requirements. Weight-based and effective rank metrics require only the task vectors and are thus the most efficient. Activation and gradient metrics require a small calibration set and forward/backward passes, but capture functional properties that pure weight-space metrics may miss.

A.5. Gradient Magnitude Regularization for Merge-Aware Finetuning

This appendix provides details on our proof-of-concept experiment investigating whether finetuning procedures informed by mergeability metrics can produce more mergeable models.

A.5.1. MOTIVATION

Our coefficient analysis identified gradient-based metrics as important predictors of mergeability. In particular, the gradient distance between task-specific models correlates with post-merge performance degradation. This suggests that models whose gradients are more aligned, or equivalently, whose parameter updates from the pretrained initialization remain similar in direction and magnitude, may be more compatible for merging.

One simple way to encourage such alignment is to regularize the magnitude of parameter updates during finetuning. By penalizing large deviations from the pretrained weights, we bias all task-specific models to remain close to the shared initialization. This keeps the models within a similar region of the loss landscape, which naturally promotes gradient alignment and reduces gradient distance between any pair of finetuned models.

A.5.2. METHOD

We augment the standard cross-entropy finetuning objective with an L_2 penalty on the parameter updates:

$$\mathcal{L}_{\text{total}} = \mathcal{L}_{\text{CE}} + \lambda \|\theta - \theta_{\text{pretrained}}\|_2^2 \quad (7)$$

where θ denotes the current model parameters, $\theta_{\text{pretrained}}$ is the pretrained initialization, and λ controls the regularization strength.

This formulation is equivalent to L_2 regularization toward the pretrained weights rather than toward zero. It encourages the finetuned model to stay close to the pretrained solution while still adapting to the downstream task.

A.5.3. EXPERIMENTAL SETUP

We finetune ViT-B/16 models on all 20 tasks in our benchmark using the same hyperparameters as the baseline (learning rate, epochs, batch size), with the addition of the gradient magnitude penalty. We evaluate three regularization strengths spanning three orders of magnitude: $\lambda \in \{0.001, 0.1, 1\}$.

After finetuning, we merge all pairwise combinations using the same four merging methods: Weight Averaging, Arithmetic merging, Task Singular Vectors (TSV), and Isotropic Merging. We report the average normalized accuracy across all 190 task pairs.

A.5.4. RESULTS

Table 12 presents the results comparing baseline finetuning against gradient magnitude regularization with different λ values.

Table 12. Effect of gradient magnitude regularization on post-merge performance. We report average normalized accuracy (%) across all 190 task pairs. Δ indicates the improvement over baseline finetuning.

Method	Baseline	$\lambda = 0.001$	Δ	$\lambda = 0.1$	Δ	$\lambda = 1$	Δ
Weight Averaging	95.86	96.11	+0.25	96.23	+0.37	96.47	+0.62
Arithmetic	91.02	91.16	+0.14	91.16	+0.14	91.74	+0.72
Task Singular Vectors	98.18	98.52	+0.33	98.51	+0.32	98.57	+0.39
Isotropic Merging	88.40	88.54	+0.15	88.58	+0.19	88.88	+0.48
Average	93.36	93.58	+0.22	93.62	+0.25	93.92	+0.55

A.5.5. DISCUSSION

The results demonstrate that gradient magnitude regularization modestly but consistently improves mergeability across all four merging methods. Key observations include:

Consistent improvements. All three λ values yield positive improvements for every merging method. The average gains increase monotonically with regularization strength: +0.22% ($\lambda = 0.001$), +0.25% ($\lambda = 0.1$), and +0.55% ($\lambda = 1$). While modest in absolute terms, the consistency across methods and the clear trend with λ suggest that the regularization is targeting a fundamental property relevant to mergeability.

Stronger regularization yields larger gains. The best results are achieved with $\lambda = 1$, the strongest regularization tested. This confirms that keeping finetuned models closer to the pretrained initialization provides meaningful benefits for mergeability, as discussed in (Zhou et al., 2025a). The monotonic improvement across three orders of magnitude of λ suggests that even stronger regularization might yield further gains, though this would need to be balanced against potential degradation in single-task performance. Conducting precise tuning of λ is beyond the scope of this experiment, intended to be a proof of concept.

Method-specific effects. At $\lambda = 1$, Arithmetic merging shows the largest improvement (+0.72%), followed by Weight Averaging (+0.62%), Isotropic Merging (+0.48%), and TSV (+0.39%). Interestingly, this ranking differs from the weaker regularization settings, where TSV and Weight Averaging benefited most. This suggests that different merging methods may have different optimal regularization strengths, opening avenues for method-specific merge-aware finetuning.

Table 13. Leave-one-task-out cross-validation results. **Left:** with L_1 penalty but without sum-to-one constraint, **Right:** the main setup of the paper, with the sum-to-one constraint and without L_1 penalty. Statistics show mean \pm std of Pearson correlation r across 20 folds.

Method	Train r	Val r	Method	Train r	Val r
Task Arithmetic	$0.572 \pm .055$	$0.448 \pm .159$	Task Arithmetic	$0.510 \pm .099$	$0.343 \pm .165$
Weight Averaging	$0.720 \pm .066$	$0.578 \pm .199$	Weight Averaging	$0.706 \pm .09$	$0.555 \pm .165$
Isotropic	$0.545 \pm .053$	$0.447 \pm .135$	Isotropic	$0.434 \pm .089$	$0.328 \pm .227$
TSV	$0.752 \pm .029$	$0.660 \pm .176$	TSV	$0.713 \pm .167$	$0.572 \pm .236$

Limitations. This experiment serves as a proof of concept rather than a comprehensive solution. The improvements, while consistent, are modest. We did not evaluate the impact on single-task performance, which may degrade with stronger regularization. More sophisticated regularization strategies that target multiple and mergeability signals, such as explicitly minimizing gradient distance to a reference model or enforcing subspace alignment during training, may yield substantially larger gains. Additionally, merge-aware finetuning strategies that incorporate knowledge of the specific merge method to be used could further improve compatibility.

Implications. These results support the broader hypothesis that mergeability is not an immutable property of task pairs but can be influenced through careful finetuning design. The pairwise metrics identified by our analysis provide actionable targets for developing more principled merge-aware training procedures.

A.6. Lasso-Regularized Linear Optimization

Besides the main linear optimization procedure detailed in the main paper, we conducted an additional experiment where the sum-to-one constraint is removed, and an L_1 penalty term is added to the loss. The purpose is to shrink the set of metrics down to a fundamental subset, removing redundant metrics. The overall loss is expressed as:

$$L = -\text{Pearson}(\text{predicted score}, \text{true performance}) + \lambda \sum_{i=1}^k |\tilde{w}^i|$$

Without additional tuning, the default value of the penalty strength coefficient λ is set to 1.

Table 13 compares the predictive performance of this sparse approach against the primary procedure detailed in the paper (unregularized, with a sum-to-one constraint). Overall, the introduction of the L_1 penalty improves predictive performance, as evidenced by higher validation correlations (r) and reduced variance. Nevertheless, **we retain the unregularized setup as our primary setting because it more effectively illuminates the relative contributions across the full spectrum of metrics**. While an L_1 penalty provides a cleaner signal by sparsifying the feature space, it can diminish the interpretability of the relative weights by pushing coefficients toward near-zero magnitudes; for instance, the distinction between coefficients of 20 and 30 is more qualitatively discernible than that between 0.002 and 0.003. Given that our objective is to uncover the underlying factors driving mergeability rather than merely engineering a superior predictor, the unregularized setup remains the most transparent diagnostic tool.

To further analyze these sparse results, we visualize both the average coefficient magnitudes and the non-zero frequency (the rate at which a metric is selected) across folds in Figure 5. On the left, the average coefficient heatmap demonstrates that most metrics become near-zero, effectively isolating the primary drivers of success. Notably, the block of effective rank metrics appears largely redundant, whereas subspace overlap and gradient-based metrics retain the highest predictive weight. This reinforces our earlier discovery regarding stable metrics: their importance persists even under strict regularization, suggesting that their contribution is fundamental rather than an artifact of collinearity. On the right, the non-zero frequency heatmap confirms this observation; effective rank metrics are consistently discarded across the 20-fold validation, while gradient and subspace metrics are selected nearly 100% of the time. Together, these complementary views demonstrate that our findings are robust to the scale and sparsity of the optimization framework.

A.7. Metric Ablation Analysis

To validate the coefficient analysis from Section 6, we perform ablation experiments where entire groups of metrics are excluded from the linear optimization.

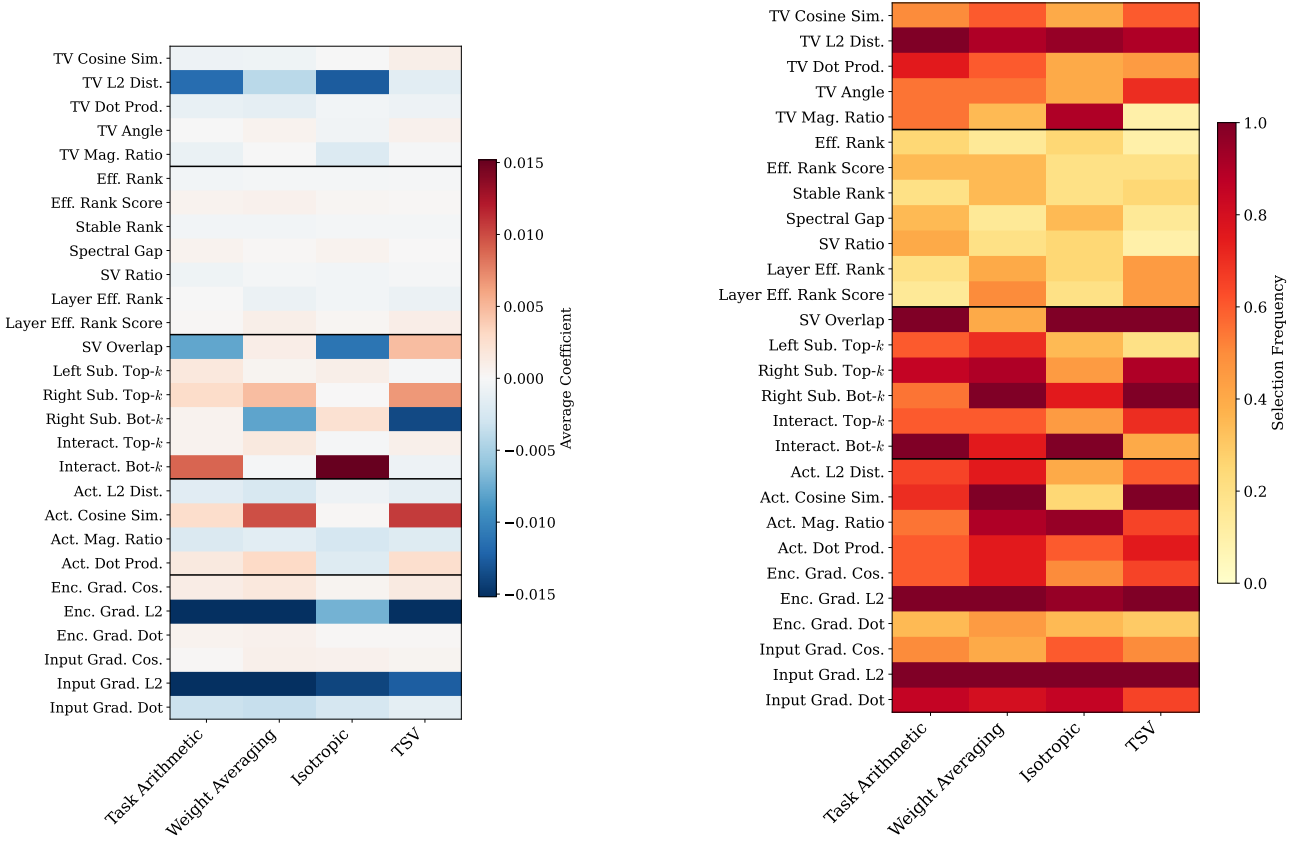


Figure 5. Left: Per-method learned coefficients for all 28 metrics, average across the 20 LOTO folds using L_1 penalty. Right: frequency of coefficients being non-zero.

A.7.1. METRIC CATEGORIES

We organize our 28 metrics into five categories:

Subspace Metrics (6 metrics): right_subspace_overlap_top_k, right_subspace_overlap_bottom_k, left_subspace_overlap, singular_value_overlap, interaction_matrix_overlap_top_k, interaction_matrix_overlap_bottom_k

Gradient-Based Metrics (6 metrics): encoder_gradient_{cosine_similarity, l2_distance, dot_product}, input_gradient_{cosine_similarity, l2_distance, dot_product}

Effective Rank Metrics (7 metrics): effective_rank, effective_rank_mergeability_score, layerwise_effective_rank, layerwise_effective_rank_mergeability_score, stable_rank, spectral_gap, singular_value_ratio

Task Vector Metrics (5 metrics): task_vector_cosine_similarity, task_vector_l2_distance, task_vector_dot_product, task_vector_magnitude_ratio, weight_space_angle

Activation Metrics (4 metrics): activation_l2_distance, activation_cosine_similarity, activation_magnitude_ratio, activation_dot_product

A.7.2. RESULTS

Table 14 illustrates the predictive performance of each ablation, compared to the baseline of retaining all 28 metrics.

Table 14. Full metric category ablation results. Validation Pearson correlation (r) reported as mean across 20 LOTO folds. Δ indicates change from baseline (full set of 28 metrics).

Method	Baseline (28)	No Subspace (-6)	No Gradient (-6)	No EffRank (-7)	No TaskVec (-5)	No Activ (-4)
Weight Avg	0.555	0.424 (-0.13)	0.399 (-0.16)	0.488 (-0.07)	0.503 (-0.05)	0.514 (-0.04)
Arithmetic	0.343	0.348 (+0.01)	0.285 (-0.06)	0.363 (+0.02)	0.394 (+0.05)	0.419 (+0.08)
TSV	0.572	0.368 (-0.20)	0.514 (-0.06)	0.603 (+0.03)	0.592 (+0.02)	0.555 (-0.02)
Isotropic	0.328	0.165 (-0.16)	0.344 (+0.02)	0.308 (-0.02)	0.314 (-0.01)	0.376 (+0.05)
Avg Δ	—	-0.123	-0.064	-0.009	+0.001	+0.017

A.7.3. ANALYSIS

Subspace and Gradient Metrics Confirm Coefficient Analysis. The ablation results align with the stable metrics identified in 6.3. Subspace metrics, including right_subspace_overlap and right_subspace_overlap_top_k, which had consistently positive coefficients, prove most critical (average $\Delta r = -0.123$). When they are excluded, TSV and Isotropic merging are particularly affected as they are based on SVD, dropping from $r = 0.572$ to $r = 0.368$ and from $r = 0.328$ to $r = 0.165$, respectively. Likewise, gradient metrics, where encoder_gradient_l2_distance and input_gradient_l2_distance had the largest negative coefficients, rank second in importance ($\Delta r = -0.064$). This confirms that the learned coefficients reflect genuine predictive importance.

Effective Rank, Task Vector, and Activation Metrics Are Largely Non-Critical. Across all methods, removing effective rank, task vector, or activation-based metrics leads to negligible changes in predictive performance when subspace and gradient-based metrics are present. In particular, effective rank metrics have minimal impact ($\Delta r = -0.009$), consistent with their near-zero coefficients in the optimization, confirming their limited relevance for mergeability prediction in this setting. Similarly, excluding task vector or activation metrics does not degrade performance, suggesting that these signals are largely redundant given the presence of stronger predictors. Overall, these results indicate that, relative to subspace overlap and gradient-based metrics, these categories contribute little additional information for predicting merge success under the considered merging methods.

A.7.4. OBSERVATIONS

Minimal Metric Set. A reduced set containing only subspace and gradient-based metrics (13 total) would carry most of the predictive power of the full 28-metric set.

Understanding Mergeability. The importance of subspace metrics suggests that mergeability is fundamentally about *geometric alignment* of learned transformations. Models merge well when their task vectors modify similar subspaces of the weight space. Gradient metrics capture complementary information about functional similarity on data.

Task Vector Metrics Are Redundant. Task vector metrics measure raw distances and angles in weight space, while subspace metrics analyze the *structured* geometric relationships (which directions are modified, not just how much). The ablation shows that this structural information subsumes the simpler distance metrics: if two task vectors have high subspace overlap, their raw distance becomes less informative for predicting merge success.

A.8. Hyperparameters

This appendix details all hyperparameters used in our experiments, including merging method configurations, metric computation settings, and optimization parameters. Let M denote the number of tasks, which is 20 in this work.

A.8.1. MERGING METHODS

Table 15 summarizes the hyperparameters for each merging method evaluated in our benchmark.

Table 15. Hyperparameters for each merging method.

Method	Parameter	Value / Description
Task Arithmetic	α (scaling)	0.3
	Formula	$\theta_{\text{merged}} = \theta_{\text{pre}} + \alpha \sum_{t=1}^M \tau_t$
Weight Averaging	α (scaling)	1.0 (implicit, no scaling)
	Formula	$\theta_{\text{merged}} = \theta_{\text{pre}} + \frac{1}{M} \sum_{t=1}^M \tau_t$
Isotropic Merging	α	1.0
TSV	SVD compression Non-matrix aggregation	Per-task (compression ratio = $1/M$) Mean

Task Arithmetic. We use a fixed scaling coefficient $\alpha = 0.3$, which has been found to work well across diverse task combinations in prior work (Ilharco et al., 2023).

Weight Averaging. It is a simple uniform average of the models and can alternatively be reduced to a special case of Task Arithmetic, where the scaling coefficient α is $\frac{1}{M}$.

Isotropic Merging. The scaling coefficient α varies depending on the number of tasks being merged. For ViT-B-16 with $M = 20$ tasks (our primary setting), we use $\alpha = 1.0$.

TSV (Task Singular Vectors). The SVD compression ratio is set to $1/M$ where M is the number of tasks being merged. Non-matrix parameters (e.g., biases, layer norms) are aggregated using the mean.

A.8.2. MERGEABILITY METRICS

Table 16 lists the hyperparameters used for computing mergeability metrics.

Subspace Overlap Metrics. For the left and right subspace overlap metrics, as well as the interaction matrix overlap, we use $k = 10$ singular directions from both the top (highest singular values) and bottom (lowest singular values) of the spectrum. This captures both the principal and residual subspaces of the task vectors. For singular value overlap, we use $k = 100$ to capture a broader distribution of the singular value spectrum.

Table 16. Hyperparameters for mergeability metric computation.

Category	Parameter	Value
Subspace Overlap	k (top/bottom directions)	10
	Singular value overlap k	100
	Applied to Layers	Left and right singular vectors All transformer blocks
Activation-Based	Calibration samples per task	10
	Batch size	32
	Random seed	42
	Target layer	visual.transformer.resblocks.11
Gradient-Based	Calibration samples per task	10
	Batch size	8
	Random seed	42
	Gradient type	Encoder and input gradients

Activation-Based Metrics. We extract activations from the last transformer block (`resblocks.11` for ViT-B-16) using 10 calibration samples per task. The activations are compared using L_2 distance, cosine similarity, magnitude ratio, and dot product.

Gradient-Based Metrics. We compute gradients with respect to both the encoder parameters and the input images. This requires a forward-backward pass on calibration data, using 10 samples per task with a batch size of 8 to manage memory constraints.

A.8.3. LINEAR OPTIMIZATION

Table 17 details the hyperparameters for the learned linear mergeability predictor.

Table 17. Hyperparameters for linear mergeability optimization.

Parameter	Value
Optimizer	Adam
Learning rate	0.01
Maximum iterations	1,000
Early stopping patience	50 iterations
Convergence threshold	10^{-4}
Metric normalization	Min-max to $[-1, 1]$
Target metric	Normalized test accuracy (average)
Cross-validation	Leave-one-task-out (20 folds)

A.8.4. MLP ABLATION

For the MLP ablation study (Appendix A.2), we used the hyperparameters reported in 18.

A.8.5. FINE-TUNING

The task-specific models were fine-tuned from a pretrained CLIP ViT-B-16 checkpoint using the hyperparameters specified by the original authors, based on convergence characteristics. See Table 19.

The number of fine-tuning epochs follows the original authors of the checkpoints on Hugging Face. Epochs vary significantly across datasets, ranging from 1 epoch for PCAM to 147 epochs for Flowers102. Full values are shown in Table 20.

Table 18. Hyperparameters for MLP mergeability predictor.

Parameter	Value
Architecture	Input → Hidden → Output
Hidden dimension	8
Activation	ReLU
Dropout rate	0.4
Optimizer	Adam
Learning rate	0.001
Weight decay (L_2)	0.001
Epochs	300
Batch size	Full batch
Input normalization	Min-max to $[-1, 1]$

Table 19. fine-tuning hyperparameters.

Parameter	Value
Base model	CLIP ViT-B-16 (OpenAI)
Optimizer	AdamW
Batch size	64
Learning Rate	$1e^{-5}$
Weight Decay	0.1
Gradient accumulation	2 steps
Gradient clipping	10.0
Precision	<i>FP32</i>
Epochs	Dataset-specific (1–147)

Table 20. Complete set of the 20 tasks and their number of fine-tuning epochs.

Task	fine-tuning Epochs
Stanford Cars	35
CIFAR10	6
CIFAR100	6
DTD	76
EMNIST	3
EuroSAT	12
FashionMNIST	5
FER2013	10
Flowers102	147
Food101	4
GTSRB	11
KMNIST	5
MNIST	5
OxfordIIIPet	82
PCAM	1
RenderedSST2	39
RESISC45	15
STL10	6
SUN397	14
SVHN	4

A.9. Datasets

Following [Gargiulo et al. \(2024\)](#), we evaluate our mergeability discovery framework on a benchmark of 20 diverse image classification tasks: SUN397 [Xiao et al. \(2016\)](#), Stanford Cars ([Krause et al., 2013](#)), RESISC45 ([Cheng et al., 2017](#)), EuroSAT ([Helber et al., 2019](#)), SVHN ([Netzer et al., 2011](#)), GTSRB ([Stallkamp et al., 2011](#)), MNIST ([Lecun et al., 1998](#)), DTD ([Cimpoi et al., 2014](#)), Flowers102 ([Nilsback & Zisserman, 2008](#)), PCAM ([Veeling et al., 2018](#)), FER2013 ([Goodfellow et al., 2013](#)), OxfordIIITPet ([Parkhi et al., 2012](#)), STL10 ([Coates et al., 2011](#)), CIFAR10 & CIFAR100 ([Krizhevsky & Hinton, 2009](#)), Food101 ([Bossard et al., 2014](#)), FashionMNIST ([Xiao et al., 2017](#)), EMNIST ([Cohen et al., 2017](#)), KMNIST ([Clanuwat et al., 2018](#)), and RenderedSST2 ([Socher et al., 2013](#)).